Analytica Chimica Acta 1337 (2025) 343553

Contents lists available at ScienceDirect

Analytica Chimica Acta

journal homepage: www.elsevier.com/locate/aca

Highly parallel simulation tool for the design of isotachophoresis experiments

Alexandre S. Avaro [a,b,1], Adar Schwarzbach [c,1], Amit Jangra [d,e], Supreet S. Bahga [d], Juan G. Santiago [a,*]

[a] Department of Mechanical Engineering, Stanford University, 488 Escondido Mall, Stanford, CA, 94305, USA
[b] ESPCI Paris, PSL Research University, LBC-CBI, CNRS UMR 8231, 10 rue Vauquelin, Paris, 75005, France
[c] Department of Computer Science, Duke University, 308 Research Drive, Durham, NC, 27708, USA
[d] Department of Mechanical Engineering, Indian Institute of Technology Delhi, Hauz Khas, New Delhi, 110 016, India
[e] Government Polytechnic, Hisar, Haryana, 125001, India

HIGHLIGHTS

- We introduce a new online simulation tool to design isotachophoresis experiments.
- The tool includes an electrolyte database and accounts for ionic strength effects.
- The tool provides an effective mobility vs. pH plot to review focusing conditions.
- Users can benchmark 972 variations of chemistry to optimize their system.
- Parallel simulations are implemented using AWS cloud computing.

GRAPHICAL ABSTRACT

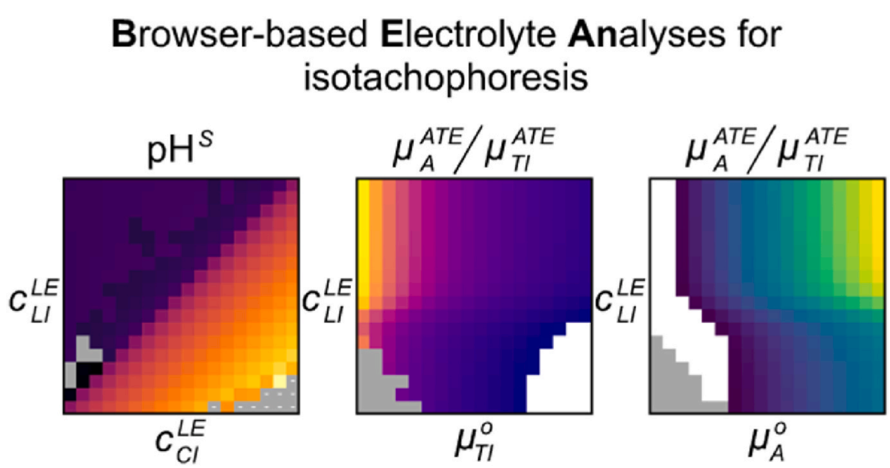

ARTICLE INFO

Keywords:
Isotachophoresis
Simulation tool
Ionic strength
Parallel computation

ABSTRACT

Background: Isotachophoresis (ITP) is a well-established electrokinetic method for separation and preconcentration of analytes. Several simulation tools for ITP have been published, but their use for experimental design is limited by the computational time for a single run and/or by the number of conditions that can be investigated per simulation run. A large fraction of the existing solvers also do not account for ionic strength effects, which can influence whether an analyte focuses in ITP. There is currently no publicly available tool for the easy and rapid design of ITP experiments.
Results: We present a rapid, highly parallelized steady-state solver for the design of buffer electrolytes in ITP experiments. The tool is called Browser-based Electrolyte Analyses for ITP (BEAN). BEAN is designed to facilitate

* Corresponding author.
E-mail address: juan.santiago@stanford.edu (J.G. Santiago).
[1] Equal contribution.

https://doi.org/10.1016/j.aca.2024.343553
Received 31 October 2024; Received in revised form 12 December 2024; Accepted 13 December 2024
Available online 17 December 2024

the evaluation and identification of functional buffer chemistries for ITP. Given a user-defined chemistry system, BEAN solves a set of coupled, non-linear integral conservation equations to determine whether a specific analyte is focused by the ITP system, and estimates quantities of interest in the design of related ITP processes. These quantities include zone concentrations, pH, and effective (observable) mobility values. BEAN also computes 972 variations of the specified ITP chemistry, including a broad range of buffer titrations and ion mobilities. All the calculations performed in BEAN include ionic strength and finite ionic radius effects, and the solver handles species with arbitrary valence. The tool further includes a searchable database of 521 commonly used electrolytes. BEAN is available at microfluidics.stanford.edu/bean.

Significance: This study introduces a novel tool that integrates known ITP steady-state equations with a highly parallel computational framework, an electrolyte database, and a web-based interface. BEAN requires no license nor compilation, and its parallel computations are performed automatically without specific implementation needed from the user. This enables users to screen wide ranges of experimental conditions in the design of ITP experiments.

1. Introduction

Isotachophoresis (ITP) is a well-established electrophoretic focusing technique applicable to a wide range of processes for the separation, purification, and/or preconcentration of analytes [1,2]. ITP focuses analytes at a self-sharpening interface between a leading electrolyte (LE) and a trailing electrolyte (TE) to create an electric field gradient that focuses target analyte ions (A). ITP also offers a method for mixing species [3] and accelerating biochemical reactions [4–6], including enzymatic reactions [7]. ITP is particularly compatible with microfluidic devices [1], including portable microfluidic systems [8].

ITP has been applied to a wide range of applications, including environmental monitoring, pharmaceuticals, food analysis, forensics, and chemical and biological detection [1,9]. The analyte focusing in ITP is governed by the relative electrophoretic mobilities of analyte, and the co-ions of leading and trailing electrolytes. Most applications and implementations of ITP involve LE and TE buffers which comprise weak electrolytes, and often involve weak electrolyte analytes, whose mobilities depend strongly on the local pH. However, the non-linear dynamics of ITP result in spatiotemporal variations in local ion concentrations and pH, which can affect the relative order of effective mobilities of various ionic species. Hence, the design of LE and TE mixtures to focus a certain analyte can require detailed computations of the pH of multi-species mixtures, including ionic strength effects on mobility and pK_a [2,5,10].

To address the complexity of ITP design, there has been significant work to develop simulation tools to help design, understand, and troubleshoot ITP processes. Simulators for electrokinetic phenomena have been reviewed elsewhere [1,11]. We here briefly distinguish between two categories of ITP simulation tools. The first consists of simple zone chemistry solvers which rely on algebraic integral form of species conservation equations coupled with chemical equilibrium relations [1,12,13]. Such tools have been used to, for example, generate so-called ITP existence diagrams. These diagrams describe the number and types of zones formed with distinct chemical makeup, and can be used to determine whether given analytes focus or not [14]. However, we know of no publicly available algebraic tool which allows for the easy or rapid design of an ITP system. The second category of solvers consists of dynamic solvers of the spatiotemporal solutions of the differential form of electromigration-diffusion-reaction conservation equations [1]. Complex partial differential equations solvers are now commonly used to precisely predict ITP concentration, pH, and electric field profiles. Popular tools include SIMUL [15], GENTRANS [16], SPRESSO [17], and more recently SPYCE [18] and CAFES [19]. These approaches offer more temporal and spatial information of ITP dynamics but can require significant time to produce an answer. This is because they are required to solve a stiff set of partial differential equations which is expensive in terms of computing power and difficult to parallelize. This limits the number of parameters and conditions which can be tested. Another limitation of current ITP simulation tools of both categories is that they are mostly limited to testing one or a small number of ITP chemistries, and this impedes assay design and optimization [1].

We here present a new platform for the design of ITP chemistries and processes. We named this tool Browser-based Electrolyte Analyses for ITP (BEAN). BEAN enables fast and parallelized computation of chemical species concentrations values in plateau-mode ITP [1]. Importantly, BEAN computes electrophoretic mobilities and dissociation constants of weak electrolytes, including ionic strength and ion valence effects. BEAN includes features to quickly explore a variety of buffer compositions for ITP, and to choose effective chemistries for a given application. The tool enables rapid estimation of whether a sample will focus within a given set of LE and TE buffer chemistries chosen by the user. BEAN also allows the evaluation of the effects of a broad range of different titrations of the LE. This includes demonstrating whether the analyte is focused, the degree to which it is preconcentrated, and the associated pH values in the sample region. We emphasize that the ITP process equations described in **section 3** are not new. Indeed, the associated theory is well established and validated [1,20,21]. The novelty of BEAN lies in the integration of these equations with a searchable database of weak electrolyte properties [22], a massively parallel computation framework, and a web-based interface, to rapidly evaluate many quantities of interest for ITP. This results in an open-source tool that enables users to test for a wide range of ITP conditions at once, and presents relevant outputs in the form of heatmaps and automated plots of given physicochemical properties.

2. Qualitative description of ITP zones and dynamics

We here present a brief qualitative summary of the various mixtures, zones, and dynamics of ITP, while a detailed description (including detailed diagrams) is given by Ramachandran and Santiago [1]. ITP focuses analyte ions (A) of a specific range of mobilities at the interface between two electrolyte mixtures. The LE contains a leading ion (LI) which has the same sign of charge as the target analyte's (a co-ion) and a mobility magnitude higher than of A. The TE contains a co-ionic trailing ion (TI) with a lower mobility magnitude. In this paper, we consider ITP systems wherein LE and TE share the same counter-ion (CI) with a charge opposite to that of LI, TI, and A. Upon application of an electric field, LI, A, and TI migrate in the same direction. This migration forms a new zone adjoining the TE which we term the adjusted TE (ATE). This zone forms in the region formerly occupied by LI but newly occupied by TI. See Fig. S2 in the **Supplementary Information (SI)** for a schematic of these dynamics.

At the interface between the LE zone (containing LI and CI) and the ATE zone (containing TI and CI), there forms a strong electric field gradient at the diffuse interface between the LI and TI. For short times, and for analytes with initially very low concentrations, the analyte focuses in so-called "peak mode", a small peak whose axial width is determined largely by the properties of the TE and LE and the applied current [1,23]. For sufficient accumulation times and sufficiently high initial analyte concentrations, the analyte focuses into a so-called "plateau mode" where the analyte is purified (relative to TI and LI) and governs the local electrical conductivity. We here term this region of purified analyte the sample zone (S). For most applications, LE, TE, and ATE are pH buffers, necessarily including one or more weak electrolytes, and many analytes are themselves weak electrolytes. All weak electrolytes have observable ion mobilities which depend strongly on local pH and the ionic strength of the electrolyte. For this reason, calculations of pH and ionic strength in all zones must be performed in order to predict whether an analyte will indeed be focused by a specific LE and TE combination. Also, if it does focus, we wish to compute the concentrations and pH of the S and ATE zones. We created BEAN in order to facilitate and speed up such calculations, including computation of many variations of buffer titration. BEAN is an open-source solver built as an easy-to-use web-based tool and can be found at the following address: microfluidics.stanford.edu/bean. We also provide the source code for BEAN at the following address: github.com/adarschwarzbach/BEAN-ITP.

3. Model description

3.1. Physico-chemical calculations

Conservation laws and governing equations to describe ITP phenomena have been extensively reviewed and applied [1,15,17]. These weak-electrolyte formulations were strongly influenced by the work of Saville and Palusinski [20]. We here summarize these equations in the case of plateau-mode ITP with four zones: TE, ATE, S, and LE. Quantities of interest for ITP experimental design are molar concentrations, pH, and effective mobilities in each zone. In turn, these quantities are a function of thermophysical parameters like fully ionized mobilities, acid dissociation constants, and relevant ion valences. We will first review the expressions for zone concentration and mobilities in the infinite dilution limit, and then review models to account for ionic strength effects.

We use the notation conventions and nomenclature of Ramachandran and Santiago [1] for ITP. In particular, μ is the electrophoretic mobility (a signed quantity; with units of $m^2/(V{\cdot}s)$), and c is the molar concentration (molar unit; e.g., M). Subscripts indicate the identity of chemical species LI, CI, A, or TI. Superscripts are used to indicate the zone of interest, among TE, ATE, S, and LE. For example, μ_A^{ATE} and c_{LI}^{LE} respectively refer to the effective mobility of the analyte ion in the ATE region, and the concentration of the leading ion within the leading electrolyte zone.

The total (analytical) concentration of a general ampholyte family X (i.e., multiple proton dissociation states of a chemical group) is given by:

$$c_X = \sum_{z=n_X}^{p_X} c_{X,z}, \tag{1}$$

where $c_{X,z}$ is the concentration of the ionic state of valence z belonging to the family X. c_X is generally a known quantity (an initial condition) within the LE and the TE. For example, LE and TE are often buffers mixed in preparation for the experiment and then introduced into a channel using pressure driven flow. n_X and p_X are respectively the minimum and maximum valence states of species X. We define the acid dissociation constant $K_{X,z}$ between valences z and $z+1$ as:

$$K_{X,z} = \frac{c_{X,z} c_H}{c_{X,z+1}}. \tag{2}$$

Here, c_H denotes the local concentration of hydronium ions H^+, such that $\mathrm{pH} = -\log_{10}\left(\frac{c_H}{1\,\mathrm{M}}\right)$. As shown by Bercovici et al. [17], the electroneutrality assumption leads to the following formulation:

$$\sum_{X=1}^{N} c_X \sum_{z=n_X}^{p_X} \frac{z L_{X,z} c_H^z}{\sum_{z'=n_X}^{p_X} L_{X,z'} c_H^{z'}} + c_H - \frac{K_w}{c_H} = 0, \tag{3}$$

where:

$$L_{X,z} = \begin{cases} \prod_{z'=z}^{-1} K_{X,z'} \text{ if } z < 0, \\ 1 \text{ if } z = 0, \\ \prod_{z'=0}^{z-1} K_{X,z'}^{-1} \text{ if } z > 0, \end{cases} \tag{4}$$

and K_w is the water dissociation constant. Equation (3) is used to calculate the pH of an electrolyte solution based on its chemical composition.

We define the effective mobility of species X, μ_X, and the local electric conductivity, σ, such that:

$$\mu_X = \sum_{z=n_X}^{p_X} \mu_{X,z}^o \frac{L_{X,z} c_H^z}{\sum_{z'=n_X}^{p_X} L_{X,z'} c_H^{z'}}, \tag{5}$$

$$\sigma = \sum_{X=1}^{N} c_X \sum_{z=n_X}^{p_X} \mathscr{F} z \mu_{X,z}^o \frac{L_{X,z} c_H^z}{\sum_{z'=n_X}^{p_X} L_{X,z'} c_H^{z'}}. \tag{6}$$

Here, $\mu_{X,z}^o$ is the fully-dissociated ionic mobility at valence z, and $\mathscr{F}$ is the Faraday number.

Plateau zone concentrations in ITP are governed by the species transport equation, which includes electromigration and diffusive fluxes. In this analysis, we ignore diffusion because it is negligible away from the sharp ITP interfaces and does not affect the ITP plateau concentrations significantly. The integral form of mass conservation for species X across an ITP zone boundary moving at constant speed V_{ITP} yields [1]:

$$V_{ITP}\left(c_X^\alpha - c_X^\beta\right) = j\left(\frac{\mu_X^\alpha c_X^\alpha}{\sigma^\alpha} - \frac{\mu_X^\beta c_X^\beta}{\sigma^\beta}\right), \tag{7}$$

Here, j denotes the current density (charge per time per area). The superscripts α and β indicate any two zones separated by an ITP zone boundary. We assume that, at steady state, the S zone does not contain LI nor TI. Similarly, we assume negligible A in the LE zone. Applying equation (7) for LI and A at the boundary between LE and S, we obtain the familiar ITP condition [1]:

$$V_{ITP} = j\frac{\mu_{LI}^{LE}}{\sigma^{LE}} = j\frac{\mu_A^S}{\sigma^S}. \tag{8}$$

Similarly, we apply equation (7) to the CI:

$$V_{ITP}\left(c_{CI}^{LE} - c_{CI}^S\right) = j\left(\frac{\mu_{CI}^{LE} c_{CI}^{LE}}{\sigma^{LE}} - \frac{\mu_{CI}^S c_{CI}^S}{\sigma^S}\right). \tag{9}$$

From equations (8) and (9), we deduce the CI concentration in S:

$$c_{CI}^S = c_{CI}^{LE} \frac{\frac{\mu_{CI}^{LE}}{\mu_{LI}^{LE}} - 1}{\frac{\mu_{CI}^S}{\mu_A^S} - 1}. \tag{10}$$

The value of c_A^S are then deduced from the values of c_{CI}^S and σ^S. We perform the same process for the ATE, which yields:

$$c_{CI}^{ATE} = c_{CI}^{LE} \frac{\frac{\mu_{CI}^{LE}}{\mu_{LI}^{LE}} - 1}{\frac{\mu_{CI}^{ATE}}{\mu_{TI}^{ATE}} - 1}. \tag{11}$$

Equations (3), (5), (10) and (11) fully describe the ITP quantities of interest in the limit of infinite dilution. Note that, unlike Jovin and Alberty conservation laws [1], this analysis is valid for arbitrary ion valences. However, these equations form a system of nonlinear implicit equations, because effective mobilities and zone conductivities depend on local concentrations. Therefore, we employ an iterative method to solve these equations. At each iteration, we use guessed values of c_A^S and c_{CI}^S to compute the local pH and effective mobilities in the S zone. This allows to update the value of c_{CI}^S using equation (10), and σ^S using equation (8). This allows to update the value of c_A^S. This process is iterated until the values of c_{CI}^S and c_A^S converge. In practice, under-relaxation at the end of each iteration improves the stability of this iterative scheme. A similar iterative scheme is used to compute species concentrations in the ATE zone.

We now describe model corrections to account for ionic strength and finite ionic radius effects. There have been extensive demonstrations of the effects of finite ionic strength on the electrophoretic mobility and the acid dissociation constants [21]. The Pitts equation is a popular correction to electrophoretic mobility in binary electrolytes. In water at 25 °C, it states the following [24]:

$$\mu^o_{X,z} = \mu^\infty_{X,z} - \left(3.1\times10^{-4}z + 0.39|z||z_{CI}|\frac{2q}{1+\sqrt{q}}\mu^\infty_{X,z}\right)\frac{\sqrt{I}}{1+0.33a\sqrt{I}}. \tag{12}$$

Here, $\mu^\infty_{X,Z}$ denotes the ion mobility at infinite dilution (expressed in $cm^2/(V{\cdot}s)$), a is the effective atomic radius given in Å, and z and z_{CI} are respectively the ion and the counter-ion valences. The ionic strength I and q are defined as:

$$I = \frac{1}{2}\sum_{X,z} z^2 c_{X,z}, \tag{13}$$

$$q = \frac{|zz_{CI}|}{|z| + |z_{CI}|}\,\frac{\mu^\infty_{X,z} + \mu^\infty_{CI,z}}{|z|\mu^\infty_{X,z} + |z_{CI}|\mu^\infty_{CI,z}}. \tag{14}$$

The Pitts formula is often regarded as a useful trade-off between accuracy and simplicity [24]. For increased accuracy, the Onsager and Fuoss model offers a more general correction for the electrophoretic mobility which is valid for an arbitrary mixture of ions. The latter can be summarized as follows [25]:

$$\mu^o_{X,z} = \mu^\infty_{X,z} - \left(A_{X,z}\mu^\infty_{X,z} + B_z\right)\frac{\sqrt{2I}}{1+aD\sqrt{I}}, \tag{15}$$

$$D = \sqrt{\frac{2e^2N_A}{\varepsilon k_B T}}, \tag{16}$$

$$A_{X,z} = z\frac{e^3}{12\pi}\sqrt{\frac{N_A}{(\varepsilon k_B T)^3}}\sum_{n=0}^{+\infty} C_n R^n_{X,z}, \tag{17}$$

$$B_z = |z|\frac{e^2}{6\pi\eta}\sqrt{\frac{N_A}{\varepsilon k_B T}}. \tag{18}$$

Here, e is the elementary charge, N_A the Avogadro number, ε is the permittivity of the solution, k_B is Boltzmann's constant, T is the temperature of the solution, and η is the viscosity of the solution. A fixed value $\frac{aD}{\sqrt{2}}$ of 1.5 $mol^{-1/2}mol^{-3/2}$ yields a good approximation for a wide range of buffers [21]. The values of C_n and $R^n_{X,z}$ are given by Onsager and Fuoss [25], and we provide in **Section S3** of the **SI** the details of this calculation applied to the mobility.

The Debye-Hückel theory yields a correction for dissociation constants of weak acids and bases. For the dissociation of an acid HA^z with valence z [21,26]:

$$\mathrm{p}K_a(I) = \mathrm{p}K_a^\infty - \log_{10}\left(\frac{\gamma_{X,z+1}}{\gamma_{X,z}\gamma_H}\right), \tag{19}$$

where:

$$\log_{10}\gamma_{X,z} = -z^2\frac{A_{DH}\sqrt{I}}{1+aD\sqrt{I}} + 0.1z^2 I. \tag{20}$$

Here, $\mathrm{p}K_a(I)$ is the $\mathrm{p}K_a$ at the ionic strength of interest, $\mathrm{p}K_a^\infty$ is the $\mathrm{p}K_a$ at infinite dilution (i.e., at $I = 0$), and $A_{DH} = 0.5102\ dm^{1/2}mol^{-1/2}$ at room temperature. $\gamma_{X,z}$ is the molar scale activity coefficient, which quantifies the departure of the activity from the ideal behavior for the species X in valence state z.

3.2. Input parameters and thermophysical properties

The basic inputs for BEAN computations are the species which make up LE and TE. Fig. 1 depicts the input panel of BEAN. First, the user selects a chemical species for each of the relevant ions (LI, CI, A, and TI). The user may search and select a species from among those stored in the fast-search database we include in BEAN. BEAN's database includes 521 common chemical species, including 303 weak acids, 161 weak bases,

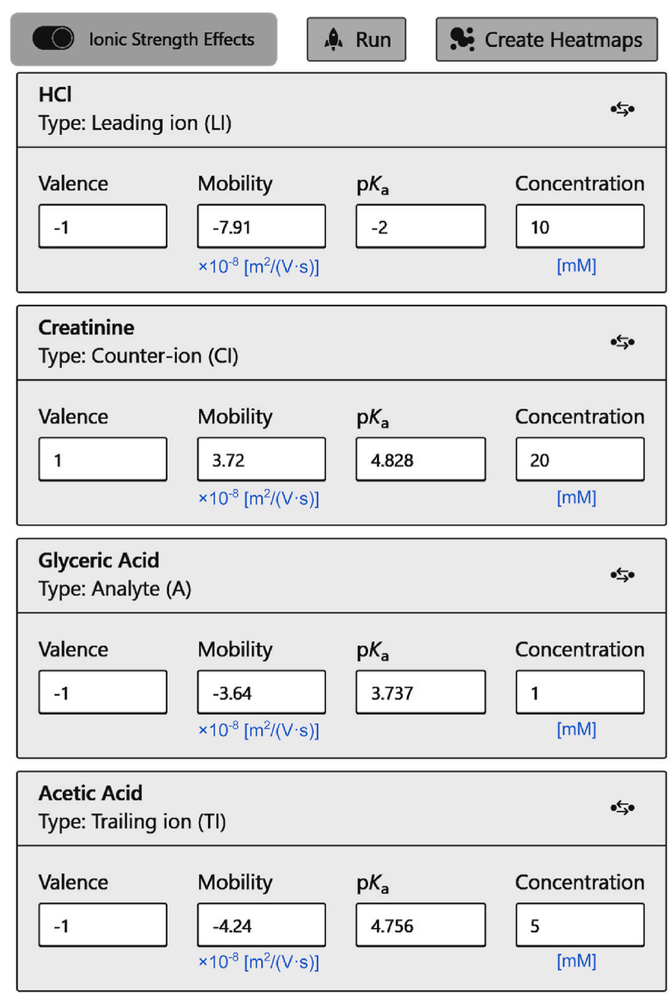

Fig. 1. Input data panel for BEAN with an example ITP chemistry. The user inputs physicochemical properties of the four ionic species (LI, CI, A, and TI). Clicking on the two-dot, opposing-arrows icon in the top right of each entry opens a window to our (optional) searchable database of 521 electrolyte species, including most buffer ions. In this example, HCl acts as the LI, creatinine as the CI, glyceric acid as the analyte ion, and acetic acid as the TI. The panel is shown here with inverted greyscale for clarity. SI units of mobility and concentration were added here in square brackets in blue text, whereas units are displayed as a tooltip (visible upon mouseover) on the website. Fully-ionized, infinite dilution mobility and $\mathrm{p}K_a$ values are taken from Ref. [27]. (For interpretation of the references to color in this figure legend, the reader is referred to the Web version of this article.)

and 57 ampholytes [19,27–31]. In addition, the user can create custom species by specifying mobilities and one (or more) pK_a values along with the relevant valence state(s). As shown in Fig. 1, each of the selected ions has a dedicated panel on the input interface. In this example, chloride ion (listed as HCl) is the LI, creatinine (a lactam commonly used as counterion for ITP [1,27,32], soluble up to roughly 0.7 M [33]) is the CI, glyceric acid (a sugar acid) is the A, and acetic acid (a common weak acid buffer ion) is the TI. These LI, TI, and A have previously been used in isotachophoresis assays [34].

For each ion, at least four physicochemical quantities must be specified by the user. These are valence, fully ionized mobility (at infinite dilution), pK_a, and analytical concentration (again, the sum of concentrations for the species family across all its valence states). Mobilities are specified as 10^{-8} m^2/(V·s) and concentrations in mM. SI units are displayed with a mouseover operation. If the user selects a species from our database, the input fields corresponding to valence, mobility, and pK_a are automatically populated with the corresponding values. If there exist multiple relevant valences for a given species, values of the physicochemical quantities for each of the valence states should be entered in the same field separated with commas. The user chooses whether ionic strength effects should be included (or not) in the calculations using the toggle button on the top left of the input interface. The "Run" button initiates the calculations.

The simplest output is a table listing the zone chemistries computed for the case specified in the input panel. Table 2 shows example output zone concentrations for the inputs of Fig. 1. These data are provided by the BEAN website and reformatted here for clarity of presentation. The "Run" button initiates computation of a series of "ITP checks" for whether an analyte is successfully focused given the TE and LE. These checks consist of the following inequalities:

$$|\mu|_{LI}^{LE} > \max\left(|\mu|_{A}^{LE}, |\mu|_{TI}^{LE}\right), \tag{21}$$

$$|\mu|_{LI}^{S} > |\mu|_{A}^{S} > |\mu|_{TI}^{S}, \tag{22}$$

$$|\mu|_{TI}^{ATE} < \min\left(|\mu|_{A}^{ATE}, |\mu|_{LI}^{ATE}\right). \tag{23}$$

These three inequalities are sufficient and necessary conditions for a "stable" ITP system. We here refer to "stable ITP" if a finite injection of the analyte results in a steady analyte concentration within a zone between the TE and LE zones [13]. The results of these three checks are displayed below the zone concentration table on the BEAN website.

The next output produced by BEAN is a computation of the effective mobility of all selected ions as a function of pH. Fig. 2 shows the computed effective mobilities versus pH for the inputs shown in Fig. 1. This plot of mobility dependence on pH for all species are designed to help the user evaluate various titrations (pH and ionic strength variations) of the LE and TE ions which may yield workable pH values of the LE.

Importantly, the tool further enables evaluation of a large number of buffer variations for each combination of chemical species. The "Create Heatmaps" button initiates 972 parallel independent simulations, whose results are displayed in the form of three heatmaps. Table 1 summarizes the various parameters that are varied in these parallel calculations, and the displayed quantity of interest, for each heatmap. Fig. 3D–F shows example output heatmaps for the inputs shown in Fig. 1. We note that even though LI and CI concentrations are varied from 1 mM to 1 M, some relevant species may not be soluble over this range. The variations of mobility values associated with the first two heatmaps is designed to help the user estimate alternate chemical species and LE zone titrations which are variations of the nominal (input) chemistry. For example, a workable range of TI mobilities can be compared to select values from the species database. For simplicity, the computations assume the mobility ranges for candidate alternate species apply to A and TI species with at most one pK_a. If relevant, this pK_a applies to an ionization state transition between −1 and 0 (weak acid) or between 0 and +1 (weak base). The third heatmap assumes only the species mobilities and pK_a of the input case, and consider wide variations in titration of the LE buffer. ITP chemistries obtained using these heatmaps should therefore be considered estimates which are subsequently validated and computed more precisely using the explicit computations associated with the Zone Concentrations table.

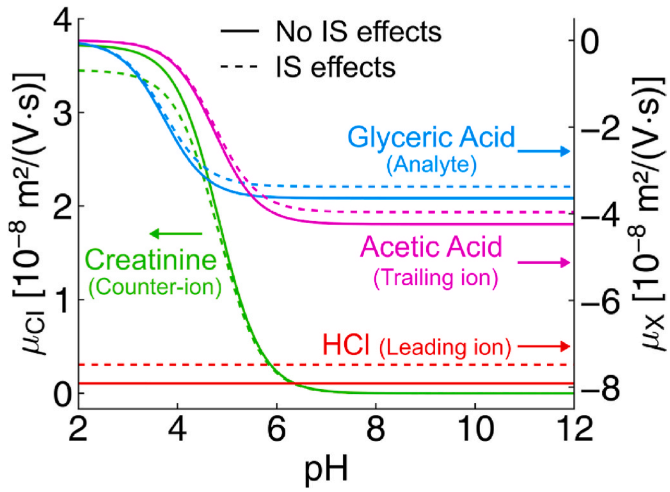

Fig. 2. Mobility of user-selected ions as a function of pH without (solid curves) and with (dashed curves) ionic strength corrections. TI, A, and LI mobilities are on the right ordinate, whereas CI mobility is on the left ordinate. Ionic strength effects are specific to buffer ion species and ionic strength. As a nominal reference, we plot corrections for the ionic strength of the ATE computed by the solver (here I_{ATE} = 5.54 mM) for A, TI, and CI, and for the ionic strength of the LE (I_{LE} = 9.74 mM) for the LI. Similar curves are provided by BEAN as line plots where a mouseover operation shows precise values of ordinate and abscissa for each point.

Table 1
Overview table of the parameters and quantities of interest of the heatmaps for BEAN.

	Heatmap 1	Heatmap 2	Heatmap 3
Quantity of interest	pH in the sample region pH^S	A-to-TI mobility ratio in the ATE $\frac{\mu_A^{ATE}}{\mu_{TI}^{ATE}}$	
Abscissa parameter	CI concentration in the LE c_{CI}^{LE}	TI absolute mobility μ_{TI}^{o}	A absolute mobility μ_{A}^{o}
Abscissa range	1 mM to 1 M	Anionic ITP: -5×10^{-8} to -1×10^{-8} m^2/(V·s) Cationic ITP: 1×10^{-8} to 5×10^{-8} m^2/(V·s)	
Ordinate parameter	LI concentration in the LE c_{LI}^{LE}		
Ordinate range	1 mM to 1 M		

Table 2
Example computed plateau concentrations and pH table for inputs of Fig. 1 including ionic strength effects. Concentrations are specified in mM for each of the zones (columns: TE, ATE, S, and LE) and for each ion (LI: HCl, CI: creatinine, A: glyceric acid, TI: acetic acid). pH values for each zone are reported in the last row.

	TE	ATE	Sample	LE
HCl	0	0	0	10
Creatinine	20	17.8	17.2	20
Glyceric Acid	0	0	7.15	0
Acetic Acid	5	7.75	0	0
pH	5.44	5.18	5.05	4.87

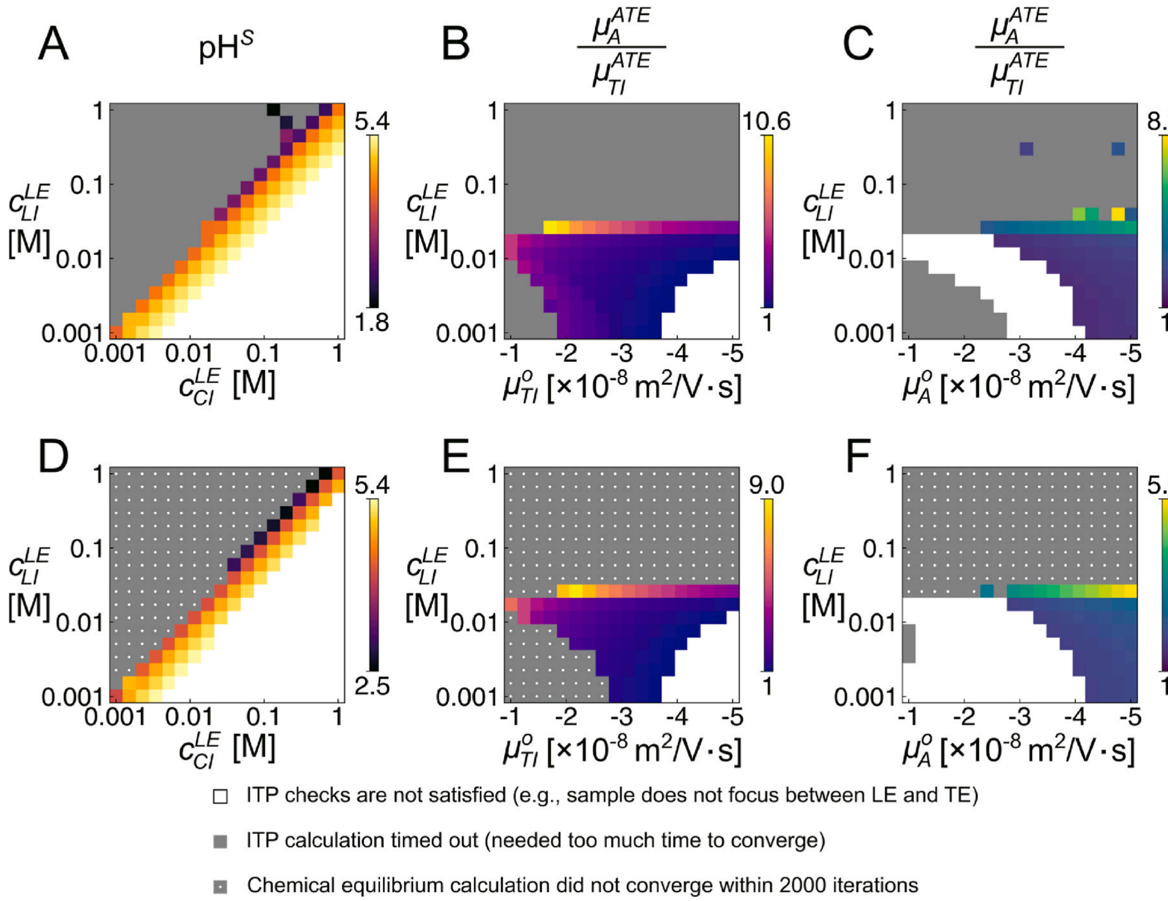

Fig. 3. Heatmaps provided by the BEAN website. The heatmaps show results of 972 parallel runs of BEAN to estimate workable variations (including candidate A and/or TI species) of the input ITP chemistry. **A** to **C** show results at infinite dilution, and **D** to **F** show results with ionic strength corrections. The heatmaps display pH in the sample region (**A**, **D**), and A-to-TI mobility ratio in the ATE (**B**, **C**, **E**, **F**). As indicated, the parameters varied are LI concentration in the LE (all heatmaps); CI concentration in the LE (**A**, **D**); fully ionized, infinite-dilution TI mobility (**B**, **E**); fully ionized, infinite-dilution A mobility (**C**, **F**).

3.3. AWS implementation

The 972 parallel runs of the calculation are implemented using AWS cloud computing services. We here provide a brief summary and plan to report a more detailed description of the computational architecture in the future. Briefly, the tool uses AWS services, including Lambda, Lambda Layers and API Gateway, coupled with Python libraries (NumPy), to run the parallel runs of the ITP simulation and create three heatmaps. We estimate with PyPAPI [35] that each “Create Heatmaps” execution in BEAN requires roughly 5.0×10^9 floating point operations if ionic strength effects are included in the calculation, and 9.1×10^8 if they are not. With the current implementation, this requires less than 30 s from the time the user requests the heatmap generation to the time the heatmaps are displayed on the website. We estimate that the same calculation would take over 1700 s (~60 times longer) to run using the best personal computers currently available for the general public.

4. Results

4.1. Rapid plateau concentration calculation & ITP checks

As mentioned, the simulation tool website provides a table of the molar concentration for each species and in each zone. Table 2 shows an example output using the inputs of Fig. 1. The LE (respectively TE) is composed of LI (respectively TI) and CI. Concentrations in the ATE and S regions are computed using the aforementioned conservation laws and chemical equilibria relations (eqs. (10) and (11)). As part of this, fully ionized mobilities and pK_a values are corrected for ionic strength effects using respectively the Onsager-Fuoss correction (eqs. (15)–(18)) and the Debye-Hückel formula (eqs. (19) and (20)). pH values for each of the zones are also reported in the last row of Table 2.

4.2. Effective mobility plot calculation

The tool then provides a plot of the effective mobilities of the relevant species as a function of pH, using equation (5), with varying c_H. Fig. 2 shows plots of example mobility computations using the inputs from Fig. 1. The website has a similar plot, and the data is plotted here in a more compact form for clarity. Anion mobilities (TI, A, and LI) are plotted on the right ordinate, and cation (CI) mobility is shown on the left ordinate. Solid curves indicate mobilities in the infinite dilution limit, and dashed curves indicate mobilities corrected for ionic strength effects; here, for simplicity, using the Pitts formula (equation (12)) and the Debye-Hückel correction (equations (19) and (20)). The values required for these calculations include ionic strength, ion valence, counter-ion valence, and infinite dilution pK_a values. As nominal, relevant values, the plots correspond to local mobilities within the specified ATE for the TI, A, and CI ions, and within the LE for the LI. Note that similar plots have been reported for the design of ITP experiments with specific analytes [29–31], but the latter references did not consider ionic strength corrections. BEAN provides a general tool to generate this plot for all analytes and includes corrections for ionic strength and species valence.

In the example of Fig. 2, the LI is chloride (a strong electrolyte) whose effective mobility is insensitive to pH. Conversely, TI, CI, and A are weak electrolytes with valence and mobility which are strong functions of pH. Specifically, TI, A, and CI have two possibly relevant valence states ((0, 1) for CI, and (−1, 0) for TI and A). Plateaus in these mobility curves typically correspond to pH regions where one valence state is dominant over the other valence states. Transitions between plateaus typically occur near pH $= \mathrm{p}K_a$. Stable ITP occur in pH ranges where the magnitude of the effective mobility of A is bracketed by those of LI and TI. In the example shown in Fig. 2, this condition is only met for pH < 5.5 in the infinite dilution case. At higher pH, no stable ITP is predicted. Note that the cutoff pH value(s) depends on the ionic strength of the ATE.

For a fixed pH, the effective mobility magnitude of species decreases when ionic strength effects are considered. As described by Bahga et al. [21], this reduction is due to two effects related to the counter-ionic atmosphere surrounding each ion. The first is associated with the polarization between the ion and its counter-ions (lowering local electric field); and the second is the additional drag experienced by the ion due to the opposing electromigration of its counterions.

Good estimates of effective mobilities are important for ITP experimental design. Indeed, ITP can only occur if, and only if, all of the mobility checks (equations (21)–(23)) are satisfied. These constraints have a major influence on the experimental design of ITP experiments. For instance, finding a pH range that is workable (i.e., wherein all mobility checks are satisfied) for a given analyte has a direct impact on the choice of the $\mathrm{p}K_a$ of the buffering counterion. Further, mobility values strongly influence other quantities relevant to ITP, including rates of ion accumulation, plateau concentrations, and plateau lengths.

4.3. Heatmaps

BEAN enables the user to evaluate a large number of variations of the specified buffer ions using three heatmaps. Fig. 3 shows two example sets of output heatmaps demonstrating possible variations of the ITP chemistry inputs shown in Fig. 1. The top row, Fig. 3A, B, and 3C, show computed variations without ionic strength correction. The bottom row, Fig. 3D, E, and 3F, show corresponding results including ionic strength correction. For each set of three heatmaps, each of the 972 pixels corresponds to one run of the simulation (as opposed to the single simulation initiated with the "Run" button). For each heatmap, two of the input parameters are varied over 18 values, resulting in 324 combinations of input parameters. The latter variations make up the abscissa and the ordinate of the heatmap, and the map intensities are outputs. Within each heatmap, all other input parameters remain fixed and equal to the value specified by the user in the input panel. White pixels indicate cases where at least one of the ITP checks (equations (21)–(23)) is not satisfied. Grey pixels indicate instances where the run timed out (>22 s). We set this timeout limit to comply with the timeout limit of the AWS API gateway of 29 s. We also specify with a white dot the cases where the root finding routine for the chemical equilibrium computation did not converge within 2000 iterations, and this is strong evidence of poor buffering conditions.

We first note that the operational envelopes found by the solver are relatively narrow, and this is reflected in the relatively small regions of valid ITP cases across all heatmaps. These envelopes are shown in Fig. 3 with colored pixels (i.e., neither white nor grey pixels). We here purposely chose an ITP chemistry which has a relatively narrow operational range. The LI is a strong titrant to the weak base CI. As is typical for such an arrangement, the pH in the S (and ATE) zones is then close to the $\mathrm{p}K_a$ of the CI provided the LI-to-CI analyte concentration ratio is within an order of magnitude of 0.5. For LI-to-CI analytical concentrations further from 0.5, the pH can vary quickly and we lose the ability to buffer [26]. More importantly, we chose here an analyte which has a relevant $\mathrm{p}K_a$ near that of the $\mathrm{p}K_a$ of the CI. Hence, significant variations of the LE zone pH quickly result in failure of ITP to focus and/or the solver to converge–resulting in the narrow operational envelopes. In **Section S4** of the **SI**, we present results for an ITP chemistry which is much more robust to variations, and therefore exhibits much wider operational envelopes.

We next discuss details of the heatmaps for each of the three columns of Fig. 3. Heatmaps **3A** and **3D**, in the first column, show the pH in the S region as a function of c_{CI}^{LE} and c_{LI}^{LE} in the abscissa and ordinate, respectively. These heatmaps clearly show the narrow operational range of c_{LI}^{LE} for this ITP chemistry. Note the workable cases found by the solver occupy the approximately well-buffered region where the LI-to-CI concentration ratio is close to 0.5. The latter region occurs approximately within the antidiagonal region of the heatmap. Cases in the upper left corner of the heatmap correspond to cases where the LI concentration is significantly larger than the CI concentration, which are poorly buffered cases in which the CI is nearly fully ionized by the strong acid LI. Cases in the lower right corner of the heatmap correspond to cases where the sample pH is larger than about 5.5. In this regime, consistent to the results of Fig. 2, the effective mobility magnitude of A is lower than that of TI and condition (22) is not satisfied. Finally, pH not only strongly affects mobility (c.f. Fig. 2), but it is itself a crucial quantity in the design of biochemical separation, preconcentration, and reaction applications. For instance, protein activity and solubility are strong functions of local pH [36].

Heatmaps **3B** and **3E**, in the second column, show A-to-TI mobility ratio in the ATE zone, as a function of infinite-dilution, fully dissociated TI mobility (abscissa) and c_{LI}^{LE} (ordinate). The populated intensity region shows a range of candidate TI mobilities for which the ITP conditions are met and which are tractable for the solver. As expected, for fixed c_{LI}^{LE}, the mobility ratio decreases with increasing TI mobility. TI mobilities larger than a cutoff mobility value result in unstable ITP, wherein at least one of the conditions of equations (21)–(23) is violated. Similarly, c_{LI}^{LE} larger than a cutoff concentration value for a given TI mobility results in unstable ITP. As expected for this chemistry, c_{LI}^{LE} strongly influences ATE chemistry and pH, and therefore strongly influences the effective mobilities of A and TI in the ATE. As discussed previously, glyceric acid only focuses if pH < 5.5. Values of c_{LI}^{LE} larger than about 20 mM (given the other concentrations given in Fig. 1) result in a poorly buffered system. Increasing the value of the buffering counterion (here, creatinine) results in a larger critical value for c_{LI}^{LE}. Interestingly, low $|\mu_{TI}^{o}|$ and c_{LI}^{LE} also result in poorly buffered systems. We attribute this to the fact that low values of $|\mu_{TI}^{o}|$ and c_{LI}^{LE} yield large $c_{CI}^{ATE}/c_{TI}^{ATE}$, disrupting the balance of buffering in the ATE. Lowering CI concentration in the LE zone mitigates the latter issue. Heatmaps **3B** and **3E** facilitate the identification of TI candidates that can focus the specified analyte among a wide range of LI titrations.

Heatmaps **3C** and **3F**, in the rightmost column of Fig. 3, show the A-to-TI mobility ratio in the ATE zone as a function of the mobility of fully dissociated, infinite-dilution mobilities for A (abscissa) and c_{LI}^{LE} (ordinate). Values of this ratio greater than unity satisfy equation (23). For a fixed c_{LI}^{LE}, the mobility ratio increases monotonically with candidate analyte mobility, as expected. For the cases computed here (but not always), the mobility ratio increases with LI concentration. For this configuration, we note that analytes with mobility magnitudes between about 2.5×10^{-8} m^2/(V·s) and 4×10^{-8} m^2/(V·s) focus only if c_{LI}^{LE} is within a narrow operating range. For example, overly high values of c_{LI}^{LE} result in a loss of buffering and unstable ITP, as discussed above. On the other hand, overly low c_{LI}^{LE} results in pH > 5.5 in either S or ATE, which leads to a violation of conditions (22) or (23). Heatmaps **3C** and **3F** help users identify analytes that can be focused using the nominal ITP chemistry specified by the user, and across a significant range of LI titrations.

As mentioned in the **section 3**, the calculations of the heatmaps **3B**, **3C**, **3E**, and **3F** assume at most univalent species. This has two important implications. First, the heatmap computations are most useful and most general for the common case of buffering species with a single relevant (or most important) $\mathrm{p}K_a$ for a given application. Second, for buffer systems with two or more $\mathrm{p}K_a$ values in the useful pH ranges, the user should select the nominal input case carefully to explore the pH range(s) of most interest. The choice of a pH range may be straightforward in some applications as pH is often dictated by the analyte of interest. Again, we recommend using the heatmaps as a first rough estimation to determine working ranges of LI concentration and mobilities for the chemistry of interest. More precise and ad hoc estimations should then be computed using the more general single-point "Run" calculations of BEAN.

Finally, it should be noted the heatmaps also serve as an instructional tool for users who are novice in the use and design of ITP systems. By leveraging the parallel computation of AWS, a large number of ITP configurations may be visualized simultaneously. This provides insights about the relationships among species concentrations, pH, mobility, and sample plateau concentration.

5. Conclusion

We developed and implemented a new web-based simulation tool for the design of ITP buffer chemistries. BEAN first facilitates the rapid evaluation of an ITP chemistry system for a given application. The tool determines whether a given analyte focuses given the LE and TE chemistries provide by the user. If the analyte successfully focuses, it quickly provides estimates of the plateau concentration and pH values of each ITP zone. BEAN also offers an evaluation of 972 variations of the specified ITP system (including buffer titrations). BEAN is integrated with a searchable database of 521 weak electrolyte chemistries, including common buffer ions. We showed example results of BEAN with glyceric acid as a model analyte ion. BEAN computations can consider the effects of ionic strength and arbitrary mixture valences. An important limitation of the tool is that it only provides plateau concentration values, and no information on the spatial distribution of the species (e.g., estimates of plateau zone lengths). We therefore recommend BEAN as an initial, rapid evaluation of feasible ITP chemistries for an application. Once a small number of chemistries is chosen, then the user should turn to a more comprehensive partial differential equation solvers such as SIMUL, SPRESSO, SPYCE or CAFES (another free, browser-based tool) for more complete spatiotemporal information, including plateau widths, ion (including analyte) accumulation rates, and the unsteady formation of zones.

CRediT authorship contribution statement

Alexandre S. Avaro: Writing – review & editing, Writing – original draft, Validation, Software, Investigation, Formal analysis, Conceptualization. **Adar Schwarzbach:** Writing – review & editing, Writing – original draft, Validation, Software, Investigation. **Amit Jangra:** Writing – review & editing, Validation, Software, Investigation, Formal analysis. **Supreet S. Bahga:** Writing – review & editing, Validation, Supervision, Software, Resources, Investigation, Funding acquisition, Formal analysis, Conceptualization. **Juan G. Santiago:** Writing – review & editing, Writing – original draft, Validation, Supervision, Methodology, Funding acquisition, Formal analysis, Conceptualization.

Declaration of competing interest

The authors declare the following financial interests/personal relationships which may be considered as potential competing interests: Juan G. Santiago reports financial support was provided by Bosch LLC. If there are other authors, they declare that they have no known competing financial interests or personal relationships that could have appeared to influence the work reported in this paper.

Acknowledgements

A.S.A. and J.G.S. gratefully acknowledge financial support from Bosch LLC.

Appendix A. Supplementary data

Supplementary data to this article can be found online at https://doi.org/10.1016/j.aca.2024.343553.

Data availability

Data will be made available on request.

References

[1] A. Ramachandran, J.G. Santiago, Isotachophoresis: theory and microfluidic applications, Chem. Rev. 122 (2022) 12904–12976, https://doi.org/10.1021/acs.chemrev.1c00640.
[2] A. Rogacs, L.A. Marshall, J.G. Santiago, Purification of nucleic acids using isotachophoresis, J. Chromatogr. A 1335 (2014) 105–120, https://doi.org/10.1016/J.CHROMA.2013.12.027.
[3] P. Smejkal, D. Bottenus, M.C. Breadmore, R.M. Guijt, C.F. Ivory, F. Foret, M. Macka, Microfluidic isotachophoresis: a review, Electrophoresis 34 (2013) 1493–1509, https://doi.org/10.1002/ELPS.201300021.
[4] F. Paratore, T. Zeidman Kalman, T. Rosenfeld, G.V. Kaigala, M. Bercovici, Isotachophoresis-based surface immunoassay, Anal. Chem. 89 (2017) 7373–7381, https://doi.org/10.1021/acs.analchem.7b00725.
[5] R. Khnouf, C. Han, Isotachophoresis-enhanced immunoassays: challenges and opportunities, IEEE Nanotechnol. Mag. 14 (2020) 6–17, https://doi.org/10.1109/MNANO.2020.2966028.
[6] M. Bercovici, C.M. Han, J.C. Liao, J.G. Santiago, Rapid hybridization of nucleic acids using isotachophoresis, Proc. Natl. Acad. Sci. U.S.A. 109 (2012) 11127–11132, https://doi.org/10.1073/pnas.1205004109.
[7] A. Ramachandran, D.A. Huyke, E. Sharma, M.K. Sahoo, C. Huang, N. Banaei, B. A. Pinsky, J.G. Santiago, Electric field-driven microfluidics for rapid CRISPR-based diagnostics and its application to detection of SARS-CoV-2, Proc. Natl. Acad. Sci. U. S.A. 117 (2020) 29518–29525, https://doi.org/10.1073/pnas.2010254117.
[8] G.V. Kaigala, M. Bercovici, M. Behnam, D. Elliott, J.G. Santiago, C.J. Backhouse, Miniaturized system for isotachophoresis assays, Lab Chip 10 (2010) 2242–2250, https://doi.org/10.1039/C004120C.
[9] P. Gebauer, Z. Malá, P. Boček, Recent progress in capillary ITP, Electrophoresis 28 (2007) 26–32, https://doi.org/10.1002/ELPS.200600396.
[10] C. Eid, J.G. Santiago, Isotachophoresis applied to biomolecular reactions, Lab Chip 18 (2017) 11–26, https://doi.org/10.1039/C7LC00852J.
[11] W. Thormann, R.A. Mosher, Dynamic computer simulations of electrophoresis: 2010–2020, Electrophoresis 43 (2022) 10–36, https://doi.org/10.1002/ELPS.202100191.
[12] J.L. Beckers, F.M. Everaerts, Isotachophoresis: the qualitative separation of cation mixtures, J. Chromatogr. A 68 (1972) 207–230, https://doi.org/10.1016/S0021-9673(00)88777-4.
[13] A. Jangra, S. Shriyam, J.G. Santiago, S.S. Bahga, A neural network model for rapid prediction of analyte focusing in isotachophoresis, Electrophoresis 45 (2024) 599–608, https://doi.org/10.1002/ELPS.202300198.
[14] P. Gebauer, P. Bocek, Zone order in isotachophoresis the concept of the zone existence diagram and its use in cationic systems, J. Chromatogr. 261 (1983) 49–65.
[15] B. Gaš, P. Bravenec, Simul 6: a fast dynamic simulator of electromigration, Electrophoresis 42 (2021) 1291–1299, https://doi.org/10.1002/ELPS.202100048.
[16] W. Thormann, C.X. Zhang, J. Caslavska, P. Gebauer, R.A. Mosher, Modeling of the impact of ionic strength on the electroosmotic flow in capillary electrophoresis with uniform and discontinuous buffer systems, Anal. Chem. 70 (1998) 549–562, https://doi.org/10.1021/ac970513x.
[17] M. Bercovici, S.K. Lele, J.G. Santiago, Open source simulation tool for electrophoretic stacking, focusing, and separation, J. Chromatogr. A 1216 (2009) 1008–1018, https://doi.org/10.1016/J.CHROMA.2008.12.022.
[18] S.S. Bahga, P. Gupta, Electrophoresis simulations using Chebyshev pseudo-spectral method on a moving mesh, Electrophoresis 43 (2022) 688–695, https://doi.org/10.1002/ELPS.202100279.
[19] A.S. Avaro, Y. Sun, K. Jiang, S.S. Bahga, J.G. Santiago, Web-based open-source tool for isotachophoresis, Anal. Chem. 93 (2021) 15768–15774, https://doi.org/10.1021/acs.analchem.1c03925.
[20] D.A. Saville, O.A. Palusinski, Theory of electrophoretic separations. Part I: formulation of a mathematical model, AIChE J. 32 (1986) 207–214, https://doi.org/10.1002/AIC.690320206.
[21] S.S. Bahga, M. Bercovici, J.G. Santiago, Ionic strength effects on electrophoretic focusing and separations, Electrophoresis 31 (2010) 910–919, https://doi.org/10.1002/ELPS.200900560.
[22] T. Hirokawa, Y. Kiso, Isotachophoretic determination of mobility and pKa, by means of computer simulation, J. Chromatogr. 252 (1982) 33–48, https://doi.org/10.1016/S0021-9673(01)88397-7.
[23] G. Garcia-Schwarz, M. Bercovici, L.A. Marshall, J.G. Santiago, Sample dispersion in isotachophoresis, J. Fluid Mech. 679 (2011) 455–475, https://doi.org/10.1017/JFM.2011.139.
[24] A. Persat, M.E. Suss, J.G. Santiago, Basic principles of electrolyte chemistry for microfluidic electrokinetics. Part II: coupling between ion mobility, electrolysis, and acid-base equilibria, Lab Chip 9 (2009) 2454–2469, https://doi.org/10.1039/b906468k.

[25] L. Onsager, R.M. Fuoss, Irreversible processes in electrolytes. Diffusion, conductance, and viscous flow in arbitrary mixtures of strong electrolytes, J. Phys. Chem. 36 (1932) 2689–2778, https://doi.org/10.1021/j150341a001.

[26] A. Persat, R.D. Chambers, J.G. Santiago, Basic principles of electrolyte chemistry for microfluidic electrokinetics. Part I: acid-base equilibria and pH buffers, Lab Chip 9 (2009) 2437–2453, https://doi.org/10.1039/b906465f.

[27] T. Hirokawa, M. Nishino, N. Aoki, Y. Kiso, Y. Sawamoto, T. Yagi, J.I. Akiyama, Table of isotachophoretic indices: I. Simulated qualitative and quantitative indices of 287 anionic substances in the range pH 3–10, J. Chromatogr. A 271 (1983) D1–D106, https://doi.org/10.1016/S0021-9673(00)80225-3.

[28] T. Hirokawa, M. Nishino, Y. Kiso, Isotachophoretic determination of mobility and pKa by means of computer simulation: II. Evaluation of m0 and pKa of 65 anions, J. Chromatogr. A 252 (1982) 49–65, https://doi.org/10.1016/S0021-9673(01)88397-7.

[29] T. Hirokawa, S. Kabayashi, Y. Kiso, Isotachophoretic determination of mobility and pKa by means of computer simulation: III. Evaluation of mobility and pKa of fifteen nucleotides and seven phosphorus oxoacids and their isotachophoretic separation, J. Chromatogr. A 318 (1985) 195–210, https://doi.org/10.1016/S0021-9673(01)90681-8.

[30] T. Hirokawa, T. Gojo, Y. Kiso, Isotachophoretic determination of mobility and pKa by means of computer simulation: IV. Evaluation of m0 and pKa, of twenty-six amino acids and assessment of the separability, J. Chromatogr. A 369 (1986) 59–81, https://doi.org/10.1016/S0021-9673(00)90099-2.

[31] T. Hirokawa, T. Gojo, Y. Kiso, Isotachophoretic determination of mobility and pKa by means of computer simulation: V. Evaluation of m0 and pKa of twenty-eight dipeptides and assessment of separability, J. Chromatogr. A 390 (1987) 201–223, https://doi.org/10.1016/S0021-9673(01)94374-2.

[32] S.G. Hjalmarsson, F.M. Everaerts, Capillary isotachophoresis, C R C, Crit. Rev. Anal. Chem. 11 (1981) 261–352, https://doi.org/10.1080/10408348108542743.

[33] S.H. Yalkowsky, Yan He, Parijat Jain, Handbook of Aqueous Solubility Data, second ed., CRC Press, Boca Raton, FL, 2010.

[34] L. Křivánková, F. Foret, P. Gebauer, P. Boček, Selection of electrolyte systems in isotachophoresis, J. Chromatogr. 390 (1987) 3–16, https://doi.org/10.1016/S0021-9673(01)94355-9.

[35] F. Loison, M. Boutigny, PyPAPI, flozz.github, 2017 io/pypapi/. (Accessed 18 July 2024).

[36] D. Voet, J.G. Voet, Biochemistry, fourth ed., 2011.